Proceedings of the 5th International Conference on Advances in Energy Research and Applications (ICAERA 2024)
Lisbon, Portugal- November 21 - 23, 2024
Paper No. 131
DOI: 10.11159/icaera24.131

Comparison of Stratification Performance in Oil-based Thermal Storage Tank for Different Immersed Discharging Coil Configurations

Anas A.E Ahmed[1], Rudrodip Majumdar[2], Sandip K. Saha[1]
[1]Indian Institute of Technology Bombay
Powai-400076, Mumbai, India
anas_ahmed@iitb.ac.in; sandip.saha@iitb.ac.in
[2]EECP, National Institute of Advanced Studies
Bengaluru-560012, India
rudrodip@nias.res.in

Abstract - This study investigates the thermal stratification characteristics of a single-medium sensible heat storage tank. The thermal energy storage (TES) system under investigation comprises a vertical cylindrical tank fitted with an immersed discharging coil. The study considers three different discharging coil configurations (helical, conical, and inverted conical). A commercial silicone oil (Hytherm 600) is used as the heat storage medium in the tank, and water serves as the discharging fluid. The thermal characteristics during the simultaneous charging and discharging operation are investigated considering a fixed charging temperature of 90 ℃, an oil flow rate of 1.25 L/min, and two different discharging flow rates (water), 0.5 and 2 L/min, respectively. Results indicate enhanced thermal performance for the helical discharging coil at the discharging flow rate of 2 L/min, with a total discharged energy of 3536.8 kJ, and a discharging efficiency of 54.1%. The highest energy discharged (3546.5 kJ) is realized in the case of the inverted conical coil. However, the losses are higher for this storage configuration, leading to a slightly reduced discharging efficiency (53.6%). The thermocline thickness broadens with increasing water flow rates through the discharging coil side. Eventually, the initial thermocline splits to form a stabilized thermocline thickness of 100 mm in the upper section of the tank for a 2 L/min coil flow rate.

***Keywords*:** Sensible heat storage, Silicone oil, Thermal stratification, Coil geometries, Heat transfer characteristics

1. Introduction

Energy storage is a useful technology for effective energy conservation, regulation, and utilization, and its importance is growing with the increasing penetration of variable renewable energy (VRE) sources in the global energy mix. Solar energy continues to be a dominant, clean, and abundant source for harnessing heat and electricity among the various green and sustainable sources identified globally. Diurnal and seasonal intermittencies in solar irradiation often cause a temporal mismatch between the energy availability and load-side demand [1], [2]. Thermal energy storage (TES) technology offers a well-established and highly adaptable solution to tackling this issue, especially from the heat dispatch point of view. Single-tank sensible heat storage systems reduce capital costs by about 30% compared to traditional two-tank systems [3], [4], [5]. However, continued efforts toward improving the thermal stratification behaviour within the TES are necessary to ensure enhanced harnessing features accompanied by high thermodynamic quality. Published literature predominantly outlines the optimization of the storage tank geometry and the development of improved immersed discharge coil configurations as possible pathways for TES performance enhancement. Yaici et al. [6] reported that a greater aspect ratio of the cylindrical TES results in improved thermal stratification. To efficiently harness the accumulated heat from the storage tank, recent storage systems utilize a cold-water stream that flows through the discharge coil immersed in the tank. The configuration of immersed discharging coils substantially affects the thermal stratification across the height of the TES tank. Positioning the discharging coil in the upper section of the tank with an upward coil configuration facilitates a higher rate of heat extraction [7], [8], [9]. Majumdar et al. [7], [10] used serpentine coil configuration in the computational study to demonstrate its superior performance compared to conventional helical coils. Purandare et al. [11] experimentally analyzed the thermal performance of conical coils with varying cone angles, and the results indicated that the helical coils have the maximum efficacy. Conte et al. [12] numerically analyzed the thermal efficiency of helical and conical coils to conclude that the conically-coiled pipe

exhibited greater heat transfer rates for the same pipe surface area. The present study focuses on a single-medium (silicone oil), single-tank TES under a simultaneous charging and discharging (SCAD) mode. Water and glycol-water mixes are widely used as working fluids in storage systems due to their cost-effectiveness and considerable heat capacity [13], [14]. However, the present investigation utilizes Hytherm 600 as the energy storage medium due to its wider operating temperature range (up to 220 °C) compared to water. Additionally, Hytherm 600 is reportedly devoid of solidification and corrosion issues. The novelty of the present numerical study pivots around the detailed comparative analysis of SCAD characteristics for three different configurations (helical, conical, and inverted conical) of the discharging coil immersed inside the cylindrical TES tank. A three-dimensional numerical model has been developed for simulating SCAD operation, considering temperature-dependent thermophysical properties of silicone oil.

2. System Description

A vertical cylindrical tank TES with an aspect ratio (H/D) of 3.86 is considered. The height of the storage tank, the inner and the outer diameter are 965 mm, 250 mm, and 256 mm, respectively. All numerical simulations in this study are performed for a fixed charging temperature of 90 °C, considering a fixed tank-side charging flow rate (oil) of 1.25 L/min. The three discharging coil configurations considered in the study have the same surface area exposed to the surrounding fluid. They also have the same inner and outer diameters, and height. The geometrical parameters of the different discharging coil configurations are presented in **Table 1**. The schematic of the immersed coil-aided cylindrical TES tank is shown in **Figure 1**.

Table 1: Geometrical parameters for different discharging coil configurations.

Parameters	Helical coil	Conical coil	Inverted conical coil
Inner diameter (m)	0.010	0.010	0.010
Outer diameter (m)	0.014	0.014	0.014
Surface area (m^2)	0.00038	0.00038	0.00038
Height (m)	0.295	0.295	0.295
Axial Pitch (m)	0.0295	0.0295	0.0295
Radial Pitch (m)	-	0.0054	0.0054
Number of turns	13	10	10
Top diameter of the coil (m)	0.120	0.10	0.220
Bottom diameter of the coil (m)	0.120	0.220	0.10

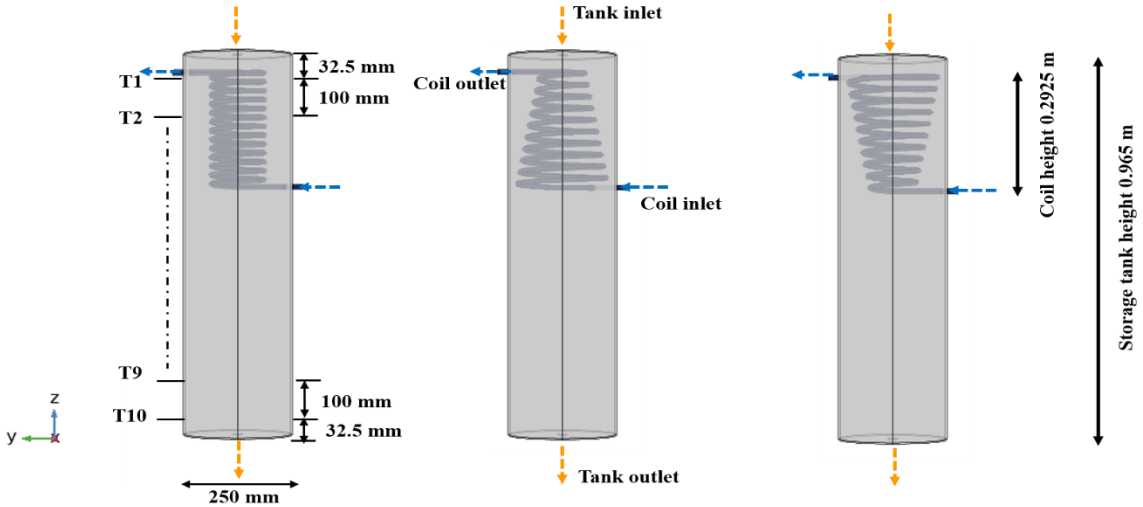

(a) (b) (c)

Fig. 1: Schematic diagram of the TES tank with (a) helical, (b) conical, and (c) inverted conical immersed discharging coil.

3. Numerical model

A three-dimensional CFD model is developed and simulated in the COMSOL Multiphysics v5.5 platform using the PARDISO solver. The convergence criteria for momentum and energy equations are 10^{-3} and 10^{-6}, respectively. Based on the precision of results, the low *Re* Number k-ε turbulent model is chosen to simulate the specified cases. It offers the advantage of simulating the buoyancy effect by activating the full buoyancy option in COMSOL [15]. Using the governing equation along with initial and boundary conditions mentioned in [15], and by incorporating the experimentally derived temperature-dependent thermophysical properties of oil using developed correlations (Eqs. (1) - (4)), detailed numerical simulations are performed. The temperature-dependent thermal conductivity of Hytherm 600 oil is imbibed from the reported literature [16]. The three-dimensional numerical model is developed based on the following assumptions: (i) Incompressible and Newtonian fluid, (ii) Thermophysical properties of the fluid are considered to be isotropic, (iii) There is no heat generated internally, (iv) Radiative heat transfer is not considered, (v) Boussinesq approximation is used to model oil density. The temperature-dependent properties of Hytherm 600 oil are as follows:

$$\boldsymbol{\mu(T)} = 0.0972 - 0.002145\boldsymbol{T} + 1.705\times10^{-5}\,\boldsymbol{T^2} - 4.668\times10^{-8}\,\boldsymbol{T^3} \quad (Pa.s) \tag{1}$$

$$\boldsymbol{\rho(T)} = 861.64 - 0.5889\boldsymbol{T} \quad (kg/m^3) \tag{2}$$

$$\boldsymbol{Cp}(\boldsymbol{T}) = 2254.9 - 2.2284\boldsymbol{T} + 0.025\boldsymbol{T^2} \quad (J/kg.K) \tag{3}$$

where, $\boldsymbol{\mu}$, $\boldsymbol{\rho}$, and $\boldsymbol{Cp}$ are dynamic viscosity, density, and specific heat capacity, respectively. The above correlations have an average R^2 of 0.97. The average thermal expansion coefficient of Hytherm 600 oil is experimentally found to be $\boldsymbol{\beta_{oil}}$ = 0.00158 ± 0.00003 (K^{-1}). The temperature-dependent thermal conductivity, i.e., $\boldsymbol{k(T)}$, is given as:

$$\boldsymbol{k(T)} = -0.0346 + 0.0007\boldsymbol{T} \quad (W/m.K) \tag{4}$$

3.1. Numerical validation

One specific experiment (***Case V***) is performed ($T_{charging}$ = 50 °C, $\dot{V}_{charging}$ = 0.5 L/min, $\dot{V}_{discharging}$ = 0.5 L/min) to validate the numerical model. The details of the TES tank, the helical coil parameters, and the experimental setup are described in a previous study [17]. The charging-alone phase for *Case V* is 1000 s, and SCAD operation takes place during *t* = 1000+ to 3000 *s* based on the tank volume. The charging time for a specific charging flow rate and TES tank volume is calculated based on the charging criteria, with the hot zone of working fluid covering approximately 70-90% of the coil height and 50% of the tank capacity. The numerical model mimics the actual conditions prevailing during the experiment. The initial temperature of the tank is fixed at 26.5 ± 0.5 °C, while the initial temperature of water at the coil inlet is 27.5 ± 0.5 °C. The ambient temperature is taken as 24.5± 0.5 °C, and convective heat transfer from the tank wall is considered. **Figure 2** shows the temporal variation of oil temperature at eight distinct axial positions of thermocouples during SCAD operation for *Case V*. A comparison of the experimental data with the numerical results shows the largest deviation in the oil temperature as ±1.78 °C. The numerical model accurately captures the time-varying patterns of the local oil temperatures, with the maximum deviation against the experimental value being 7.57%. The experimental uncertainties associated with the temperature, the charging flow rate, and the discharging flow rate are ± 0.5 °C, 0.75%, and 1%, respectively.

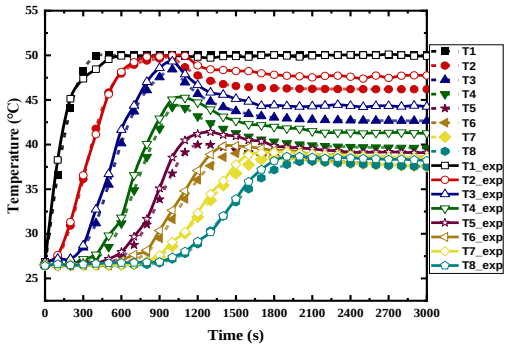

Fig. 2: Temporal variation of oil temperature obtained from the experiments and numerical simulations for *Case V*.

3.2. Grid size and time step independence test

The grid size independence study uses three different mesh sizes: **Mesh 1** (152102 elements), **Mesh 2** (395091 elements), and **Mesh 3** (960807 elements). The outlet temperature of the discharging coil is chosen to ascertain the grid independence since it is directly related to the amount of energy extracted from the TES tank. **Figure 3(a)** depicts the temporal variations in the coil outlet temperature for *Case V*. While moving from Mesh 1 to Mesh 2, the maximum error between the numerical results and the experimental data reduces substantially from 9.8% (Mesh 1) to 7.57% (Mesh 2). However, the computational cost increases with an increase in the number of elements by a factor of 2.59. Upon moving from Mesh 2 to Mesh 3, the reduction in error is not significant compared to the computational cost, since the trial error obtained with Mesh 3 is 6.83%. Thus, considering both computational efforts and accuracy, Mesh 2 (395091 elements) is used for the case study simulations. The time step independence study examines three different time steps (1 *s*, 5 *s*, and 10 *s*), as illustrated in **Figure 3(b)**. Using Mesh 2, there is no substantial difference in coil outlet temperature across multiple time steps. Therefore, the intermediate time step of 5 *s* has been selected for further simulations.

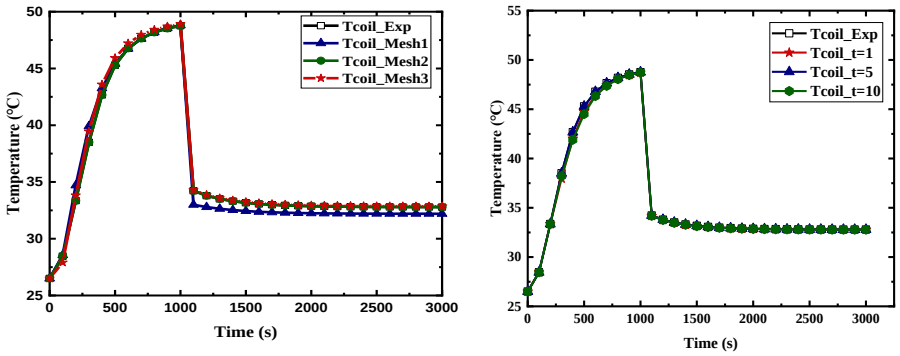

(a) (b)

Fig. 3: (a) Grid independence and (b) time step independence studies.

3.3. Operating conditions

To investigate the stratification phenomena in the oil during the simultaneous charging and discharging (SCAD) operation using three different coil configurations, the parametric conditions defined in **Table 2** are used. The investigation considers a coil-side discharging flow rate (water) lower than the tank-side charging flow rate (oil), leading to the addition of 0.5 L/min discharging rate among the considered cases. The lower flow rate (i.e., a longer residence time of water inside the coil) allows for more energy extraction and necessitates further examination of thermal stratification on the oil side. The charging time (1200 *s*) for the predefined oil flow rate is calculated based on the charging criteria mentioned before, and the oil density. At the end of the charging-alone phase, the coil is completely covered by the hot zone of the oil (i.e., an axial distance of 482.5 mm measured from the top of the TES tank).

Table 2: Operating conditions used in the numerical model to simulate SCAD operation.

Case	Coil	Discharging water flow rate (L/min)	Operation time (s)	
			Charging	SCAD
A1	Helical	0.5	1200	1200^{+} to 3600
A2	Helical	2	1200	1200^{+} to 3600
B1	Conical	0.5	1200	1200^{+} to 3600
B2	Conical	2	1200	1200^{+} to 3600
C1	Inverted conical	0.5	1200	1200^{+} to 3600
C2	Inverted conical	2	1200	1200^{+} to 3600

4. Results and discussion

4.1. Thermal performance characteristics

For comparative evaluation of the TES tank configurations of interest, the temporal variation of oil temperature inside the storage tank, water temperature at the coil outlet, energy stored inside the TES tank during the SCAD operation, total energy discharged by the coil, the rate of energy discharge, discharging efficiency and the thermocline thickness are used as the metrics. The mathematical expressions for these parameters, including analyses of energy stored within the tank wall and energy lost to the ambient, are available in a previously reported study [18].

4.2. Temporal variation of the storage and discharging medium

Figures 4(a)-(c) demonstrate the temporal variations in temperature profiles for all the investigation instances (*see* **Table 2**). Temperature measurements are performed using ten thermocouples (*T1-T10*). In each case, the TES tank is charged by the oil heated at 90 ℃ during t = 0-1200 *s*. During TES charging, temperatures captured by thermocouples *T1-T4* rise steeply in all the *Cases*. The temperatures captured by *T5* and *T6* rise toward the end of the charging phase as the heat diffuses toward the bottom section of the TES tank. The SCAD process occurred during t = 1200 - 3600 *s*. **Figures 4(a)-(c)** show a significant drop in temperatures *T2-T4* following the commencement of the SCAD operation, and the reduction is more pronounced for the larger flow rate (i.e., 2 L/min) through the discharging coil, owing to the enhanced heat extraction by the coil. The temperature *T1* remains unfazed over the whole operation, owing to its proximity to the tank entrance. The rise in temperatures *T5-T8* is curbed by an increase in the water flow rate through the discharging coil, owing to a reduced heat diffusion toward the tank bottom.

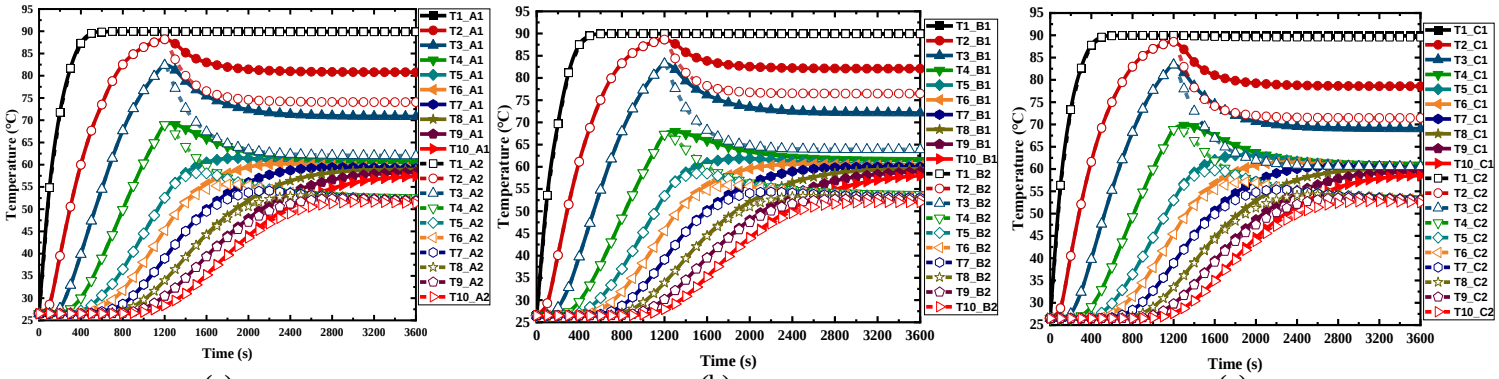

(a) (b) (c)

Fig. 4: Temporal variation of oil temperature for *Cases* (a) *A1* and *A2*, (b) B1 and *B2*, and (c) *C1* and *C2*.

4.3. Temporal variation of the coil outlet temperature and energy content

Figure 5(a) depicts the temporal variations in the coil outlet temperature for all the investigation instances (see **Table 2**). During the charging phase (t = 0 - 1200 *s*), the static water within the coil absorbs energy from the TES tank, raising the temperature of the encapsulated water close to the charging temperature. With the commencement of the SCAD operation at t = 1200 *s*, a fresh flow of cold water (T= 27.5 ℃) enters the coil, leading to a sharp drop in the coil outlet temperature as the encapsulated hot water is suddenly displaced. A lower discharging flow rate (water) of 0.5 L/min results in a higher coil outlet temperature attributable to a higher residence time of circulating water within the immersed discharging coil. **Figure 5(b)** shows the temporal evolution of the cumulative energy discharged by the coil in all the cases. The energy discharged increases with an increase in the discharging flow rate.

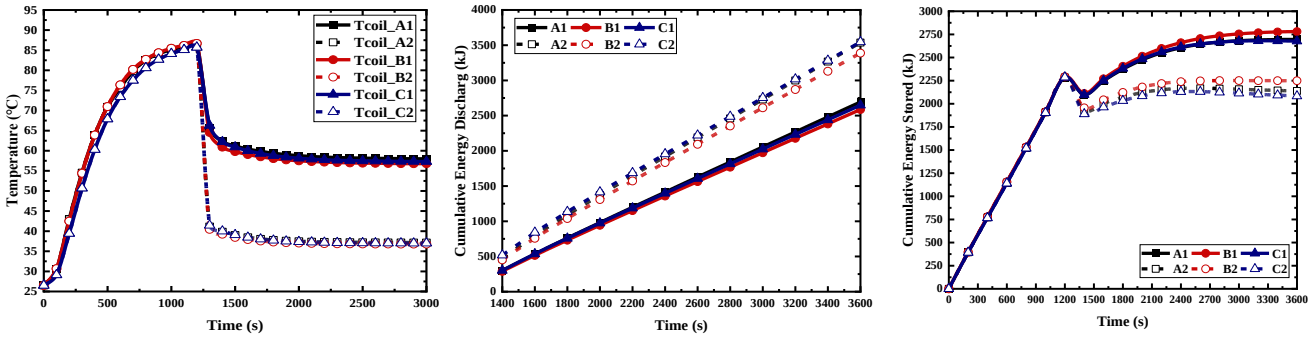

(a) (b) (c)

Fig. 5: Temporal variation of (a) Coil outlet temperature (b) cumulative energy discharged and (c) cumulative energy stored.

Figure 5(c) depicts the temporal variations in cumulative energy stored in the TES for all the cases. The energy stored in the storage tank increases over time as the heat is constantly supplied by the incoming hot oil. However, an abrupt reduction in total energy stored is observed for all the cases following the commencement of SCAD operation. This drop indicates that the instantaneous thermal energy released from the tank is more than the instantaneous energy input. Furthermore, Cases *A2* and *C2* exhibit higher energy discharged and lesser energy stored owing to enhanced energy extraction from the TES tank.

4.4. Temporal variation of energy discharged performance and thermocline

Figure 6(a) exhibits that the rate of energy discharged is proportional to the coil flow rate in all the cases. During the initial stage of SCAD operation, a significant temperature difference is observed across the coil terminals. However, the temperature at the coil outlet becomes almost constant with time following the sharp drop at the commencement of SCAD operation, leading to energy discharge at a constant rate. **Figure 6(b)** depicts the temporal variation of discharging efficiency for the different cases considered. The discharging efficiency assumes a zero value during the charging duration because of no flow through the coil. Commencement of the SCAD operation causes a rapid increase in discharging efficiency. As time progresses, the net energy available within the TES tank is reduced, which is also reflected by an improvement in discharge efficiency. The discharge efficiency becomes constant once the storage system approaches the state of thermal equilibrium. **Figure 6(c)** exhibits that the primary thermocline continues to expand at an average rate of 0.33 mm/s until t = 1500 *s*. The rapid degradation of the thermal gradient across the tank height is attributable to the high convective losses to the ambient. *Cases A2* and *C2* correspond to the highest rate of energy discharged, maximum value of average discharging efficiency, and the highest primary thermocline thickness of 600 mm.

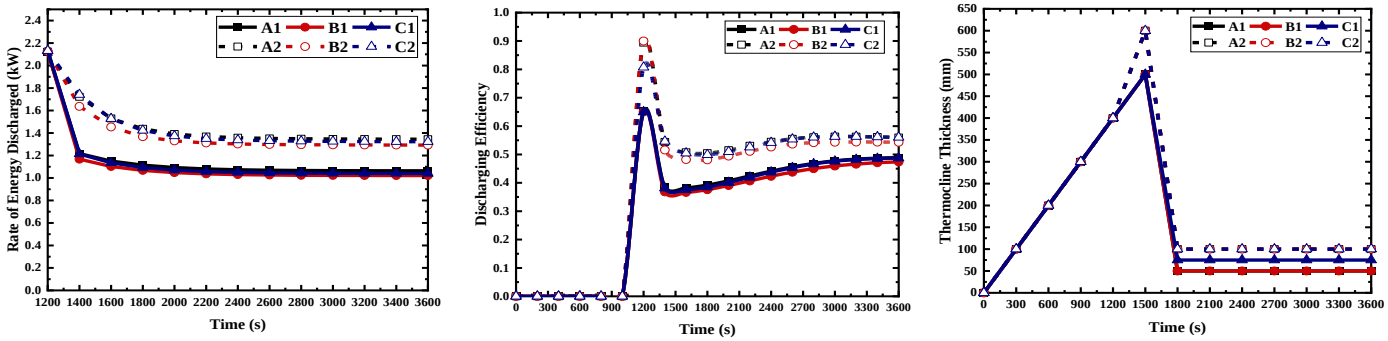

(a) (b) (c)

Fig. 6: Temporal variation of (a) Rate of energy discharged, (b) discharging efficiency, and (c) thermocline thickness.

Table 3 shows the energy analysis for all the cases, summarizing the net energy input, cumulative energy discharged, average discharging efficiency, cumulative energy stored, and energy losses (combined value of the energy captured by the wall, and energy lost to the ambient) during the operation. ***Cases A2*** and ***C2*** exhibit higher energy discharged and discharging efficiencies, indicating better energy-harnessing features for helical and inverted conical coils. Notably, the inverted conical coil presents a larger surface area to the incoming hot oil near the tank inlet.

Table 3: Energy analysis for all the investigation instances of SCAD operation.

Case	Net energy input (kJ)	Cumulative energy discharged (kJ)	Cumulative energy stored in TES (kJ, at t = 1200 *s*)	Energy lost to the tank wall and ambient (kJ) (% of Net Input)	Average discharging efficiency
A1	6670.5	2692.6	2695.6	1282.3 (18.4%)	44.3%
A2	6872.8	3536.8	2138.2	1197.7 (17.4%)	54.1%
B1	6661.2	2586	2780.2	1295 (19.4%)	42.6%
B2	6846.2	3387.7	2248.9	1209.6 (17.6%)	52%
C1	6619.9	2647.7	2676.8	1295.4 (19.5%)	44%
C2	6835.8	3546.5	2083.1	1206.2 (17.6%)	53.6%

Figure 7 exhibits the oil temperature distribution (2-D) within the TES tank for ***Cases A2***, ***B2***, and ***C2*** at two instants (i.e., t=1200 s and t=2400 *s*). The figure shows the creation of a thermocline zone caused by the buoyancy forces, prompting the hot oil (with lesser density) to settle on top of the denser and cooler oil layers. The thermocline zone broadens and sinks deeper into the storage tank with time. At *t* =1200 *s*, the thermocline thickness is close to 400 mm in all the cases. The primary thermocline thickness stabilizes following the splitting of the initial thermocline. At *t* =2400 *s*, a thermocline of 100 mm thickness is observed in the upper section of the TES in the cases with a higher water discharging flow rate of 2 L/min.

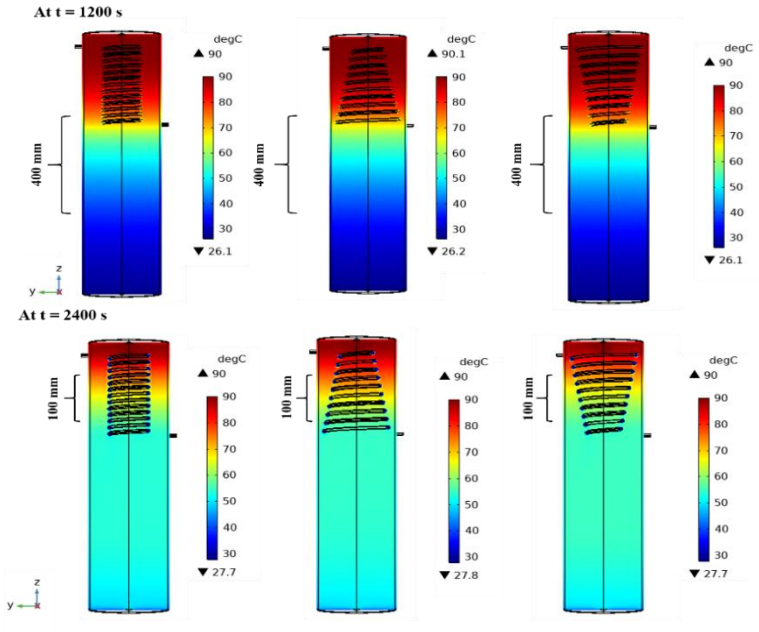

(a) (b) (c)

Fig.7: Oil temperature distribution (2-D) within the storage tank for *Cases (a) A2, (b) B2,* and (c) *C2*.

5. Conclusion

The present numerical study examines the thermal stratification characteristics of a cylindrical sensible heat storage tank under simultaneous charging and changing operation, considering three different immersed discharging coil configurations. Hytherm 600 oil is used as the heat storage medium, whereas water is used as the discharging fluid. The helical discharging coil exhibits the most effective energy extraction, followed by the inverted conical coil. The conical coil exhibits the weakest energy-harnessing features. The thermophysical properties of Hytherm 600 oil oppose the buoyancy force caused by convective heat transfer, leading to a systemic hindrance to energy extraction by the water flowing through the discharging coil. An increased water flow rate of 2 L/min through the coil demonstrates improved energy extraction and less energy accumulation in the TES tank. *Case C2* exhibits the largest value for total energy discharged (3546.5 kJ), followed

by *Case A2 (*3536.8 kJ). However, a lesser energy loss in the case of *Case A2* (1197.7 kJ) compared to *Case C2* (1206.2 kJ) leads to a slightly higher discharging efficiency for *Case A2* (54.1%), compared to *Case C2* (53.6%). Further work is needed on different geometrical shapes of oil-based TESs equipped with effective coils to ascertain the optimal TES configuration.

References

[1] A. Kumar and S. K. Saha, "Energy and exergy analyses of medium temperature latent heat thermal storage with high porosity metal matrix," Appl Therm Eng, vol. 109, pp. 911–923, Oct. 2016, doi: 10.1016/j.applthermaleng.2016.04.161.

[2] R. Majumdar, S. Singh, and S. K. Saha, "Quasi-steady state moving boundary reduced order model of two-phase flow for ORC refrigerant in solar-thermal heat exchanger," Renew Energy, vol. 126, pp. 830–843, Oct. 2018, doi: 10.1016/j.renene.2018.04.008.

[3] H. Khurana, R. Majumdar, and S. K. Saha, "Numerical investigation on the performance of the helical and conical coil heat exchanger configurations in the dynamic mode of heat extraction," in AIP Conference Proceedings, 2584, 040001(2023). doi: 10.1063/5.0134122

[4] H. Khurana, R. Majumdar, and S. K. Saha, "Improved realistic stratification model for estimating thermocline thickness in vertical thermal energy storage undergoing simultaneous charging and discharging," J Energy Storage, vol. 82, Mar. 2024, doi: 10.1016/j.est.2024.110490.

[5] R. Majumdar, S. K. Saha, and S. Singh, "Evaluation of transient characteristics of medium temperature solar thermal systems utilizing thermal stratification," Appl Energy, vol. 224, pp. 69–85, Aug. 2018, doi: 10.1016/j.apenergy.2018.04.083.

[6] W. Yaïci, M. Ghorab, E. Entchev, and S. Hayden, "Three-dimensional unsteady CFD simulations of a thermal storage tank performance for optimum design," Appl Therm Eng, vol. 60, no. 1–2, pp. 152–163, 2013, doi: 10.1016/j.applthermaleng.2013.07.001.

[7] H. Khurana, R. Majumdar, and S. K. Saha, "Formulation of prediction model for working fluid temperature in a vertical paraboloid shaped thermal energy storage tank during stand-alone operation", Proceedings of 16th International Conference on Heat Transfer, Fluid Mechanics, and Thermodynamics (HEFAT-2022), Virtual Conference, 08-10 August 2022, pp. 507-512. Available: https://www.researchgate.net/publication/362733013

[8] H. Khurana, R. Majumdar, and S. K. Saha, "Response Surface Methodology-based prediction model for working fluid temperature during stand-alone operation of vertical cylindrical thermal energy storage tank," Renew Energy, vol. 188, pp. 619–636, Apr. 2022, doi: 10.1016/j.renene.2022.02.040.

[9] H. O. Njoku, O. V. Ekechukwu, and S. O. Onyegegbu, "Analysis of stratified thermal storage systems: An overview," 2014, Springer Verlag. doi: 10.1007/s00231-014-1302-8.

[10] R. Majumdar and S. K. Saha, "Reduced order heat exchanger models for low-to-medium temperature range solar thermal applications," in Energy, Environment, and Sustainability, Springer Nature, 2019, pp. 357–393. doi: 10.1007/978-981-13-3302-6_12.

[11] P. S. Purandare, M. M. Lele, and R. K. Gupta, "Investigation on thermal analysis of conical coil heat exchanger," Int J Heat Mass Transf, vol. 90, pp. 1188–1196, Aug. 2015, doi: 10.1016/j.ijheatmasstransfer.2015.07.044.

[12] I. Conté, X. F. Peng, and B. X. Wang, "Numerical investigation of forced fluid flow and heat transfer from conically coiled pipes," Numeri Heat Transf A Appl, vol. 53, no. 9, pp. 945–965, Jan. 2008, doi: 10.1080/10407780701789948.

[13] H. Khurana, S. Tiwari, R. Majumdar, and S. K. Saha, "Comparative evaluation of circular truncated-cone and paraboloid shapes for thermal energy storage tank based on thermal stratification performance," J Energy Storage, vol. 34, Feb. 2021, doi: 10.1016/j.est.2020.102191.

[14] H. G. Kamath, R. Majumdar, A. V. Krishnan, and R. Srikanth, "Cost and environmental benefits of coal-concentrated solar power (CSP) hybridization in India," Energy, vol. 240, Feb. 2022, doi: 10.1016/j.energy.2021.122805.

[15] H. Khurana, R. Majumdar, and S. K. Saha, "Thermal stratification characteristics during simultaneous charging and discharging for different storage tank geometries with immersed discharging coil," Appl Therm Eng, vol. 225, May 2023, doi: 10.1016/j.applthermaleng.2023.120235.

[16] S. Advaith, D. R. Parida, K. T. Aswathi, K. Dani, U. K. Chetia, K. Chattopadhyay, and S. Basu, "Experimental investigation on single-medium stratified thermal energy storage system," Renew Energy, vol. 164, pp. 146–155, Feb. 2021, doi: 10.1016/j.renene.2020.09.092.

[17] Anas A.E Ahmed, R. Majumdar, and S. K. Saha, "Experimental investigation of stratified sensible thermal energy storage using silicone oil," Proceedings of the 27th National and 5th International ISHMT-ASTFE Heat and Mass Transfer Conference (IHMTC 2023), December 14-17, 2023, pp. 827-832. Available: http://dx.doi.org/10.1615/IHMTC-2023.1340

[18] H. Khurana, R. Majumdar, and S. K. Saha, "Experimental investigation of heat dispatch controllability through simultaneous charging-discharging and stand-alone discharging operations in vertical cylindrical sensible heat storage tank," J Energy Storage, vol. 54, Oct. 2022, doi: 10.1016/j.est.2022.105268.